Sciencexpress Research Article

High-Resolution View of the Yeast Meiotic Program Revealed by Ribosome Profiling

Gloria A. Brar,[1] Moran Yassour,[2,3,4] Nir Friedman,[4,5] Aviv Regev,[2,3] Nicholas T. Ingolia,[1]*† Jonathan S. Weissman[1]†

[1]Howard Hughes Medical Institute, Department of Cellular and Molecular Pharmacology, University of California, San Francisco, and California Institute for Quantitative Biosciences, San Francisco, CA 94158, USA. [2]Broad Institute of Massachusetts Institute of Technology and Harvard, Cambridge, MA 02142, USA. [3]Howard Hughes Medical Institute, Department of Biology, Massachusetts Institute of Technology, Cambridge, MA 02139, USA. [4]School of Engineering and Computer Science, Hebrew University, Jerusalem, 91904, Israel. [5]Alexander Silberman Institute of Life Sciences, Hebrew University, Jerusalem, 91904, Israel.

*Present address: Department of Embryology, Carnegie Institution for Science, Baltimore, MD, 21218, USA.

†To whom correspondence should be addressed. E-mail: ingolia@ciwemb.edu (N.T.I.); weissman@cmp.ucsf.edu (J.S.W.)

Meiosis is a complex developmental process that generates haploid cells from diploid progenitors. We measured mRNA abundance and protein production through the yeast meiotic program and found strong, stage-specific expression for most genes, achieved through control of both mRNA levels and translational efficiency. Monitoring of protein production timing revealed uncharacterized recombination factors and extensive organellar remodeling. Meiotic translation is also shifted towards noncanonical sites, including short open reading frames (sORFs) on unannnotated transcripts and upstream regions of known transcripts (uORFs). Ribosome occupancy at near-cognate uORFs was associated with more efficient ORF translation; in contrast, some AUG uORFs, often exposed by regulated 5' leader extensions, acted competitively. This work reveals pervasive translational control in meiosis and helps to illuminate the molecular basis of the broad restructuring of meiotic cells.

Sexual reproduction is enabled by meiosis, a strongly conserved cell division that generates haploid progeny from a diploid precursor. Meiosis has been studied for over a century including extensive analyses in the budding yeast *Saccharomyces cerevisiae* [reviewed in (*1*, *2*)], where it is linked to spore formation. These efforts have provided a wealth of knowledge about the movement and changes in organization of meiotic chromosomes. Far less is known about the molecular basis of the remodeling events that impact other aspects of meiotic cellular physiology. Pioneering microarray studies (*3*) provided a basic framework of molecular changes accompanying yeast meiotic progression but failed to capture many dynamic processes, in part due to extensive post-transcriptional regulation including specific instances of functionally-significant translational control [reviewed in (*2*); (*4*)]. Whether translational control plays a general role in meiotic protein production, however, is unclear.

Ribosome profiling, based on deep-sequencing of ribosome-protected mRNA fragments, allows monitoring of translation with scale, speed, and accuracy that rivals approaches for following mRNA levels (*5*, *6*). Applying this method to sporulating *S. cerevisiae* cells allowed us to follow the molecular events underlying meiosis with unprecedented depth.

A high-resolution atlas of meiotic mRNA abundance and new protein synthesis. Our studies relied on three critical features: optimized meiotic synchrony, dense timepoints that oversampled meiotic transitions, and in-depth staging of each timepoint. We collected samples through two separate meiosis experiments (Fig. 1A, 1B, fig. S1A). The first used an optimized version of traditional synchronization procedures and focused on early meiotic stages. The second timecourse used an estrogen-activatable variant of the Ndt80 transcription factor (*4*, *7*), allowing synchronous progression through the meiosis I and II (MI and MII) chromosome segregation stages (*4*). Each timepoint was staged in detail (Fig. 1B and figs. S2 and S3) and 25 of them, chosen for comprehensive meiotic coverage, were selected, along with two cycling vegetative samples, for ribosome profiling and mRNA sequencing (Fig. 1A and fig. S1A). Use of timepoints that oversampled meiotic stages allowed for synthesis of the data into a master timecourse (Fig. 1A and fig. S1B) and selective pooling, collapsing meiotic progression into 9 categories for some analyses (fig. S4).

Staging revealed a high degree of synchrony and provided a cytological framework to anchor expression data (Fig. 1B and figs. S2 and S3). Examination of ribosome footprints for specific genes showed that the sample synchrony was reflected in sharp, discrete translation patterns (Fig. 1C). The

large majority (6134 out of 6708) of genes were translated at some point in meiosis and most showed strong temporal regulation. In addition to a large shift in expression patterns between vegetative cells and cells entering meiosis, 66% of meiotically-expressed genes varied by at least 10-fold in protein synthesis level through meiotic progression itself, a range that far exceeded measurement errors (Fig. 2A and fig. S5, A-D). These changes were due largely to the meiotic program itself rather than the nutrient deprivation conditions that accompany sporulation (fig. S6).

Expression clustering to probe meiotic cell biology and gene function. Clustering of the timepoints by genome-wide protein synthesis patterns precisely recapitulated their order (figs. S1B and S6A). Thus dynamic control of protein synthesis results in unique expression signatures throughout the meiotic program. Accordingly, grouping of all genes by protein synthesis pattern through meiosis revealed numerous multifaceted clusters (Fig. 2A).

Many clusters emerged from groups of functionally-related genes. This was seen prominently for genes involved in translation, mitochondrial function, mitochondrial translation, nutrient uptake, proteasome function and redox reactions (Fig. 2A, numbered at middle panel; tables S1 and S2). Furthermore, a tight cluster of 27 proteins that were synthesized at the onset of DNA replication was predominantly composed of critical DNA replication and chromosome structure factors [Fig. 2A, top; table S2; (*8*)]. Similarly, genes involved in recombination and synaptonemal complex (SC) formation were expressed precisely when these processes occurred and emerged as a discrete group containing 46 genes from unbiased clustering of the full dataset (Fig. 2A, bottom; table S2). Notably, this cluster included the large majority of meiotic genes with characterized roles in double-strand break formation, crossover/noncrossover choice, and SC structure [reviewed in (*9–11*)].

Several uncharacterized genes were found in the recombination/SC cluster, suggesting their involvement in these intensely-studied processes (*1*). Indeed, loss of either *YDR506C* or *YLR445W* delayed nuclear division, consistent with a role for these factors in prophase, when recombination and SC formation occur (Fig. 2, B and C, and fig. S7A). *ydr506c*Δ and *ylr445w*Δ cells showed distinct, specific defects in SC morphogenesis (fig. S7, B and C) and in both cases the meiotic progression delay was largely alleviated when the recombination checkpoint was bypassed by deletion of *SPO11* (Fig. 2, B and C, and fig. S7A). The strong delay in *ylr445w*Δ cells, however, was not fully-dependent on Spo11 (Fig. 2C and fig. S7A), implying this gene has additional functions.

Evidence for cellular remodeling. While the ability to observe precise temporal regulation allowed specific co-clustering of some genes, there were prominent cases in which genes with a common function or localization showed highly disparate expression patterns. For example, we found tightly-controlled but distinct patterns of expression among endoplasmic reticulum (ER) proteins suggesting major ER remodeling events (fig. S8 and table S3). A strong downregulation (relative to vegetative cells) of a set of ER genes, including ergesterol biosynthesis components, occurred prior to meiotic induction. After meiotic entry, a broad group of ER genes were induced, including glycosylation factors (table S3). Finally, following MI, a subset of folding factors, sphingolipid biosynthetic genes, and trafficking components were upregulated. This last remodeling phase is accompanied by induction of the Unfolded Protein Response [UPR; (*12*, *13*); Fig. 1C, see also Fig. 3F below)].

Autophagy components also showed discrete patterns of expression, suggesting dynamic control of distinct autophagic processes during sporulation [fig. S9A, table S4; (*14*)]. *ATG8*, a gene central to many branches of autophagy (*15*), was expressed highly from early in the meiotic program and its deletion caused an early and profound meiotic defect (fig. S9, B and C). By contrast, *ATG32*, a mitophagy-specific factor (*16*, *17*), showed low expression until the meiotic divisions (fig. S9B). Delayed onset of mitophagy may ensure full mitochondrial function, which is needed to power early meiotic stages (*18*). Consistently, *atg32*Δ cells progressed normally past prophase, but showed delayed meiotic completion (fig. S9D).

Translational control in meiosis. Control of protein production reflects both regulation of mRNA levels and the efficiency with which these messages are translated into proteins. Measuring translation rates and mRNA levels allowed us to evaluate their relative contributions. Much transcriptional regulation was observed, but translational control also regulated the magnitude and timing of protein production in meiotic cells. An example of this interplay is provided by the adjacent *SPS1* and *SPS2* genes (Fig. 3A). mRNA for both genes accumulated late in prophase and persisted through the meiotic divisions, consistent with their transcriptional control by *NDT80* (*19*). By contrast, *SPS1*, but not *SPS2*, was strongly translationally-regulated, delaying Sps1 protein synthesis until MII (Fig. 3, A and B).

To quantitatively evaluate the role of translational control, we calculated relative translation efficiencies (TEs; ribosome footprint RPKM/mRNA RPKM; RPKM = reads per kilobase million) for messages through our timecourse. Replicates indicated high TE reproducibility (error < 20%), allowing sensitive measurement of dynamic translational control [fig. S5, E and F, (*6*)]. This approach confirmed, both in timing and degree, the strong MI-specific translational repression that regulates the B-type cyclin, *CLB3* [(*4*), Fig. 3C]. At least

ten genes showed a highly similar pattern of translational regulation as *CLB3*- including *SPS1* (Fig. 3A), *GIP1* and *SPO20*- which, like *CLB3*, have known roles only late in meiosis (*20–22*).

Genome-wide analysis revealed that meiotic translational regulation is both pervasive and nuanced (Fig. 3D). As seen for vegetative cells (*6*), meiotic cells showed strong basal differences in translation rates among genes (Fig. 3D). Globally, we observed a net decrease in translation relative to vegetative exponential cells that was most pronounced at the very earliest and latest timepoints (fig. S10). Further, gene-specific regulation was widely used to dynamically tune gene expression. For example, 24% of genes during the "core meiotic" period showed greater than 3-fold TE changes, a period during which net translation capacity appears stable (fig. S10). More than 200 genes in the full timecourse and 66 in the "core meiotic" period exhibited a dynamic range in TE that was comparable to the ~10-fold changes seen for *GCN4*, an archetype of strong translational regulation (*23*).

Changes in TE frequently correlated with timing of gene function (Fig. 3E). The DNA replication factor *ORC1* (*24*), for example, showed strong translational repression at later meiotic stages when cells do not replicate DNA. Zip1, an SC component (*25*), specifically showed poor translation in vegetative cells and spores, consistent with the lack of SC in either state. Chitin deposition factor Rcr1 (*26*), is translated efficiently only at late timepoints, concomitant with new cell wall generation. Finally, *HAC1*, the central UPR mediator (*12*, *13*), showed transient translational activation shortly upon transfer of cells to nutrient-limited conditions, followed by a later, stronger translational activation during the meiotic divisions, as cells are synthesizing new membrane and spore walls (Fig. 3F). *HAC1* is regulated translationally through cytoplasmic splicing of its message (*27*). Consistently, *HAC1* mRNA splicing mirrored TE measurements, both in timing and degree (Fig. 3F). The UPR has been heavily studied in yeast using harsh inhibitors of ER folding (e.g. DTT). This study reveals a unique opportunity to follow the UPR in a physiological setting.

Noncanonical translation. Beyond translational control of canonical open reading frames (ORFs), we also observed a shift towards noncanonical translation during the meiotic program. While vegetative cells exhibited ~5% of ribosome footprints mapping outside annotated ORFs, in meiotic cells up to ~30% of footprints mapped outside of these regions (Fig. 4A). These footprints largely mapped to discrete novel translation sites with well-defined AUG starts and stop codon stops. We systematically annotated translation units by exploiting the strong peak in ribosome density seen at translation initiation sites to identify utilized start codons [fig. S11; (*6*)]. This strategy was sensitive, allowing de novo identification of start codons for most known ORFs (fig. S12A), and specific, strongly enriching for ORFs initiating at AUG (fig. S13).

Novel ORFs were found on noncanonical mRNAs, including transcripts antisense to known ORFs, alternate transcripts at canonical loci, and transcripts in regions thought to be intergenic (Fig. 4, B and C and figs. S12A, S14, S15A). We also identified instances of genome misannoation (e.g. fig. S15B). Many newly-annotated ORFs were on stable transcripts, similar to those predicted as noncoding in a meiotic tiling array study [(*28*), fig. S14]. Our empirical strategy found translation of short ORFs (sORFs; fig. S12A) that were well-expressed (fig. S12, B and C) and highly-regulated (fig. S16), but below the cutoff of 80-100 amino acids used historically to computationally identify yeast ORFs.

Recent studies have identified cellular functions for short peptides (*29*, *30*), though the function of these meiotic sORFs remains an open question. Minimally, our data suggests the export of many novel transcripts into the cytoplasm, allowing translation by ribosomes. Conversely, this dataset facilitates identification of transcripts that act at the RNA level. For example, most antisense transcripts are poorly-translated, including *RME2* and *RME3*, antisense to *IME4* and *ZIP2* respectively, which are known to act through direct cis-transcriptional interference of their sense counterpart [figs. S12C and S17, A, B, and D; (*31*, *32*)]. By contrast, a transcript antisense to *YFL012W* that shows no transcriptional interference activity, contained prominent regions of translation [(*31*), fig. S17, C and D].

uORFs in meiosis. The second major source of novel meiotic ribosome density was leader sequences (commonly called 5' untranslated regions), situated upstream of the canonical ORFs (Fig. 4D and fig. S18A). We saw no general meiotic increase in footprints in 3'UTRs, arguing against a nonspecific increase in translational background noise. Examination of individual gene leaders revealed short footprint spans that started at either AUGs or near-cognate codons and generally spanned the region until the next stop codon (Fig. 4D and fig. S18A). Nearly 300 of such upstream ORFs (uORFs) have been identified in yeast under starvation conditions [(*6*), reviewed in (*33*)], but we found them to be far more common in meiosis.

We annotated 10,226 meiotic uORFs, present in the leaders of 3026 genes (fig. S11). These uORFs contained a density of ribosome footprints far greater than the ribosome footprint density in non-uORF leader regions, suggesting that our annotation approach was thorough and specific (fig. S19, A and B). Ribosome occupancy at uORFs was higher in meiotic than vegetative cells (Fig. 4D and figs. S18A and S19, B and C) and most of this effect derives from the meiotic program itself rather than the starvation conditions that accompany sporulation (fig. S19D). As expected, AUG,

when present, was efficiently used for uORF translation initiation. The near-cognate codons that showed most efficient initiation, UUG and CUG (fig. S18, B and C), have also been shown to be most efficient in mammalian cells and in vitro (*5*, *34*).

uORFs have been implicated in translational regulation, though no universal functional role has emerged. uORFs that have been well-characterized through reporter studies show diverse effects, either enhancing, decreasing, or having little impact on downstream ORF translation. [reviewed in (*33*)]. Three features of our study ideally positioned us to evaluate the role of uORFs in translation. First, we annotated many uORFs, allowing distillation of general principles. Second, we collected data for each timepoint on mRNA abundance and rates of translation, allowing instantaneous quantitation of TE for each downstream ORF, while traditional approaches require TE inference by steady-state protein abundance. Finally, our analysis of numerous sequential points through a dynamic process allowed detection of temporal trends. Correlations of ribosome occupancy of leaders and TE of their corresponding downstream ORFs over 10 timepoints (see fig. S4) typically revealed a strong positive relationship (Fig. 4, E and F). However, a subset of leaders containing at least one AUG uORF showed a negative correlation, suggesting a competitive relationship between uORF and ORF translation in these cases (Fig. 4F and fig. S20, see Fig. 5E below).

Leader extensions and competitive uORFs. For some messages, we found enriched footprint occupancy of leaders was caused by a programmed change in the transcript length during meiosis. Systematic analysis identified 192 genes with regulated leader length (Fig. 5, A-C; fig. S21; and table S5). For example, *ORC1*showed an extended leader after prophase. This extension revealed a number of well-translated uORFs (Fig. 5B) and was accompanied by a concurrent decrease in translation of the *ORC1* coding region (Figs. 3E and 5, B and D). Of genes with regulated leaders, a prominent subset showed a similar inverse relationship, often corresponding well with known gene function. Orc1 and Ndj1, for example, have no characterized function late in meiosis (*24*, *35*) and *RED1*, a key meiotic prophase factor (*36*), is translationally-repressed exclusively in vegetative cells (Fig. 5D).

For genes with leader extensions containing one or more AUG uORF, at least half showed a strong negative correlation between the ribosome occupancy of the leader and TE of the ORF (Fig. 5E). By contrast, for leaders containing uORFs starting only with near-cognate, non-AUG codons, this correlation was strongly positive (Fig. 5E). Regulated leaders have been observed in budding yeast and mammalian cells, with longer forms often associated with poor ORF translation (*37*, *38*). Here we have observed a far broader and more nuanced role for leader extensions in providing temporal translational control to many meiotic genes.

More generally, our analyses point to disparate roles for AUG and near-cognate uORFs (Figs. 4F and 5E). A fraction of AUG uORFs appear to competitively down-modulate ORF expression. By contrast, near-cognate uORFs are more common and show a generally strong positive correlation with expression of their downstream ORF, possibly allowing cells to divert limited resources to an important subset of messages. Whether uORFs directly prime translation of their downstream ORF is unclear. Nonetheless, genes with the strongest positive correlation between leader ribosome occupancy and ORF TE are highly enriched for known function in sporulation (table S6), suggesting physiological relevance to this regulation. The broad monitoring of gene expression by genomics has underscored the importance of quantitative modulation, beyond a model of binary on/off control. MicroRNAs provide a prominent example of developmental control through subtle regulation of broad sets of genes. uORFs may similarly allow condition-specific tuning of protein synthesis for a large portion of the genome.

The preponderance of uORFs suggests a shift of the translation initiation mechanism in meiotic cells from the predominant mechanism in which the initiation factors recognize the mRNA cap and the initiation complex scans the message for the first AUG to commence translation [reviewed in (*23*)]. A link between alternative translation initiation mechanisms and the use of uORFs is suggested by analysis of messages that were shown to support cap-independent translation in nitrogen starved yeast cells [*YMR181C*, *GPR1*, *BOI1*, *FLO8*, *NCE102*, *MSN1*, *GIC1*; (*39*)]. We found that all had leaders with well-translated near-cognate uORFs and a strong positive correlation between leader ribosome occupancy and ORF translation (Fig. 4F; fig. S22, excluding *BOI1* as it has a complicating leader extension; table S5).

Perspective. We find that even in the extensively-studied yeast, *S. cerevisiae*, genome coding has a complexity not captured by existing annotations. Ribosome profiling also captured a layer of regulation that is invisible to mRNA measurements, revealing extensive and dynamic translational regulation of canonical ORFs. Transcription studies have enabled the identification of trans-factors that control diverse cellular processes, while a similarly broad understanding of the importance and mechanisms of translational control remains elusive. This dataset provides a valuable foundation for identifying such cis- and trans- translational regulators.

This study also gives a holistic view of the metabolic and cellular reorganization seen through the yeast meiotic program, extending beyond a traditional chromosome-centric picture. Previous studies suggested that meiotic transcriptional control was limited to a few discrete waves (*3*, *40*). Our data reveal multifaceted control of protein

production, enabled by the tightly-timed induction of many translational and transcriptional programs, including those driving translation factors, the proteasome, and the UPR. Indeed, the view of such responses as environmentally-controlled stress pathways may reflect the historical context of their discovery rather than their sole physiological role.

References and Notes

1. D. Zickler, N. Kleckner, *Annu. Rev. Genet.* **33**, 603 (1999).
2. A. L. Marston, A. Amon, *Nat. Rev. Mol. Cell Biol.* **5**, 983 (2004).
3. S. Chu *et al*., *Science* **282**, 699 (1998).
4. T. Carlile, A. Amon, *Cell* **133**, 280 (2008).
5. N. T. Ingolia, L. F. Lareau, J. S. Weissman, *Cell* **147**, 789 (2011).
6. N. Ingolia, S. Ghaemmaghami, J. Newman, J. Weissman, *Science* **324**, 218 (2009).
7. K. Benjamin, C. Zhang, K. Shokat, I. Herskowitz, *Genes Dev.* **17**, 1524 (2003).
8. P. T. Spellman *et al*., *Mol. Biol. Cell* **9**, 3273 (1998).
9. A. Lynn, R. Soucek, G. Borner, *Chromosome Res.* **15**, 591 (2007).
10. S. Keeney, M. J. Neale, *Biochem. Soc. Trans.* **34**, 523 (2006).
11. S. Page, R. Hawley, *Annu. Rev. Cell Dev. Biol.* **20**, 525 (2004).
12. J. S. Cox, P. Walter, *Cell* **87**, 391 (1996).
13. K. Mori, T. Kawahara, H. Yoshida, H. Yanagi, T. Yura, *Genes Cells* **1**, 803 (1996).
14. I. Piekarska, R. Kucharczyk, B. Mickowska, J. Rytka, B. Rempola, *Eur. J. Cell Biol.* **89**, 780 (2010).
15. Z. Xie, D. J. Klionsky, *Nat. Cell Biol.* **9**, 1102 (2007).
16. T. Kanki, K. Wang, Y. Cao, M. Baba, D. J. Klionsky, *Dev. Cell* **17**, 98 (2009).
17. K. Okamoto, N. Kondo-Okamoto, Y. Ohsumi, *Dev. Cell* **17**, 87 (2009).
18. A. Jambhekar, A. Amon, *Curr. Biol.* **18**, 969 (2008).
19. S. Chu, I. Herskowitz, *Mol. Cell* **1**, 685 (1998).
20. A. M. Neiman, *J. Cell Biol.* **140**, 29 (1998).
21. H. Tachikawa, A. Bloecher, K. Tatchell, A. M. Neiman, *J. Cell Biol.* **155**, 797 (2001).
22. H. Friesen, R. Lunz, S. Doyle, J. Segall, *Genes Dev.* **8**, 2162 (1994).
23. N. Sonenberg, A. G. Hinnebusch, *Cell* **136**, 731 (2009).
24. S. P. Bell, R. Kobayashi, B. Stillman, *Science* **262**, 1844 (1993).
25. M. Sym, J. Engebrecht, G. Roeder, *Cell* **72**, 365 (1993).
26. K. Imai, Y. Noda, H. Adachi, K. Yoda, *J. Biol. Chem.* **280**, 8275 (2005).
27. C. Sidrauski, J. S. Cox, P. Walter, *Cell* **87**, 405 (1996).
28. A. Lardenois *et al*., *Proc. Natl. Acad. Sci. U.S.A.* **108**, 1058 (2011).
29. T. Kondo *et al*., *Science* **329**, 336 (2010).
30. Y. Xu, D. Ganem, *J. Virol.* **84**, 5465 (2010).
31. B. Gelfand *et al*., *Mol. Cell. Biol.* **31**, 1701 (2011).
32. C. F. Hongay, P. L. Grisafi, T. Galitski, G. R. Fink, *Cell* **127**, 735 (2006).
33. H. M. Hood, D. E. Neafsey, J. Galagan, M. S. Sachs, *Annu. Rev. Microbiol.* **63**, 385 (2009).
34. S. E. Kolitz, J. E. Takacs, J. R. Lorsch, *RNA* **15**, 138 (2009).
35. H. Y. Wu, S. M. Burgess, *Curr. Biol.* **16**, 2473 (2006).
36. B. Rockmill, G. S. Roeder, *Proc. Natl. Acad. Sci. U.S.A.* **85**, 6057 (1988).
37. J. Badhai, J. Schuster, O. Gidlof, N. Dahl, *PLoS ONE* **6**, e17672 (2011).
38. G. L. Law, K. S. Bickel, V. L. MacKay, D. R. Morris, *Genome Biol.* **6**, R111 (2005).
39. W. V. Gilbert, K. Zhou, T. K. Butler, J. A. Doudna, *Science* **317**, 1224 (2007).
40. A. P. Mitchell, *Microbiol. Rev.* **58**, 56 (1994).
41. M. Longtine *et al*., *Yeast* **14**, 953 (1998).
42. G. A. Brar, A. Hochwagen, L. S. Ee, A. Amon, *Mol. Biol. Cell* **20**, 1030 (2009).
43. R. Visintin *et al*., *Mol. Cell* **2**, 709 (1998).
44. J. Loidl, F. Klein, J. Engebrecht, *Methods Cell Biol.* **53**, 257 (1998).
45. K. Nairz, F. Klein, *Genes Dev.* **11**, 2272 (1997).
46. M. Yassour *et al*., *Genome Biol.* **11**, R87 (2010).
47. M. J. de Hoon, S. Imoto, J. Nolan, S. Miyano, *Bioinformatics* **20**, 1453 (2004).
48. M. B. Eisen, P. T. Spellman, P. O. Brown, D. Botstein, *Proc. Natl. Acad. Sci. U.S.A.* **95**, 14863 (1998).
49. A. J. Saldanha, *Bioinformatics* **20**, 3246 (2004).
50. O. R. Homann, A. D. Johnson, *BMC Biol.* **8**, 49 (2010).
51. M. Yassour *et al*., *Proc. Natl. Acad. Sci. U.S.A.* **106**, 3264 (2009).
52. T. Moll, G. Tebb, U. Surana, H. Robitsch, K. Nasmyth, *Cell* **66**, 743 (1991).
53. O. Cohen-Fix, J. M. Peters, M. W. Kirschner, D. Koshland, *Genes Dev.* **10**, 3081 (1996).
54. A. Hochwagen, A. Amon, *Curr. Biol.* **16**, R217 (2006).
55. S. Keeney, C. N. Giroux, N. Kleckner, *Cell* **88**, 375 (1997).
56. A. Bergerat *et al*., *Nature* **386**, 414 (1997).
57. F. He *et al*., *Mol. Cell* **12**, 1439 (2003).

Acknowledgements: We thank E. Ünal, A. Amon, and members of the Weissman lab for critical reading of this manuscript; C. Chu for sequencing assistance; J. Dunn for protocol development assistance; F. Van Werven for the MATa/a strain; and F. Klein for the the Zip1 antibody. GAB is supported by American Cancer Society Postdoctoral fellowship 117945-PF-09-136-01-RMC. MY is supported by a Clore Fellowship. This work was supported by a grant from the US-Israel Bi-national

Science Foundation (NF, AR), an NIH P01 (AG10770; NTI), a Ruth L. Kirschstein NRSA (GM080853; NTI), and HHMI funding (JSW, AR). A patent on the ribosome profiling approach has been assigned to the University of California. Supporting files are in the SOM and at www.ncbi.nlm.nih.gov/geo/ with Series accession number GSE34082.

Supporting Online Material

www.sciencemag.org/cgi/content/full/science.1215110/DC1
Materials and Methods
Figs. S1 to S22
Tables S1 to S7
References (*41–57*)
Files S1 and S2

10 November 2011; accepted 13 December 2011
Published online 11 December 2011; 10.1126/1215110

Fig. 1. Ribosome profiling through meiosis. (**A**) Timepoints (white lines) were taken through two overlapping timecourses. Cartoon representations of meiotic stages are below. (**B**) A subset of staging controls. Positions of staging plots correspond to timepoints in (A). (**C**) Ribosome footprints across specific genes are shown for categories in fig. S4. Y-axis scales are independent by gene.

Fig. 2. A global view of protein synthesis through sporulation. (**A**) Ribosome footprints (RPKM) were summed over each yeast gene (columns) for all samples except steady-state spores (rows). The summed expression of each gene over timepoints was normalized to 1 for the timecourse and genes were subjected to clustering. Several clusters are noted: 1. Mito. ribosome 2. Nutrient uptake, Amino acid biosynth. 3. Mito. function 4. Proteasome 5. Redox/energy generation 6. Ribosome/translation machinery. Meiotic progression is indicated pictorially to the right. The top panel shows a cluster containing genes responsible for DNA replication, with the gene identities to the right. To the left is the average footprint density across the cluster, with timepoints corresponding to bulk DNA replication represented by arrows. The bottom panel shows a cluster of genes associated with recombination and SC formation. The bar to the left shows the timing of these events as determined by staging controls. Asterisks identify genes analyzed in (B) and (C) and fig. S7. (**B**) *Wild-type*, *ydr506cΔ* and *ydr506cΔspo11Δ* cells were induced to sporulate. At indicated times, samples were scored for nuclear division. (**C**) *Wild-type*, *ylr445wΔ* and *ylr445wΔ spo11Δ* cells were induced to sporulate and treated as in (B).

Fig. 3. Widespread dynamic translational control in meiosis. (**A**) Log_2 mRNA and footprints (RPKM) for a region containing *SPS1* and *SPS2* over pooled timepoints (fig. S4). (**B**) *SPS1-3HA SPS2-FLAG* cells carrying an estrogen-inducible *NDT80* allele were induced to sporulate. At 6 hours, ß-estradiol was added. Samples from indicated times were subjected to Western and Northern blotting. (**C**) Log_2 TE values for *CLB3* and *YPT1* for pooled timepoints (fig. S4). MI and MII are indicated by colored boxes. (**D**) Cluster analysis of log_2 TE through meiosis for pooled categories (fig. S4) for all genes. (**E**) Log_2 TE are plotted as in (C) for *AMA1*, *RCR1*, *ORC1*, and *ZIP1*. (**F**) Log_2 TE are plotted as in (C) for *HAC1*. Below, total RNA from the original timecourse (see fig. S1) was subjected to Northern blotting for *HAC1*.

Fig. 4. Noncanonical translation is pervasive in meiotic cells. (**A**) Footprints from pooled timepoints (see fig. S4) were mapped. The percent of these footprints outside of known ORF annotations is plotted. (**B**) mRNA and ribosome occupancy profiles around *YOL092W*, with sense above the line for each timepoint and antisense below. * denotes the sORF start site. The 'AUG unit' (sORF) was annotated by the strategy in S11. (**C**) The region around *SAS4* is displayed as in (B), with truncated ORF start denoted by *. (**D**) Ribosome occupancy profile for vegetative and meiotic cells over the leader of *ACB1*. (**E**) For pooled timepoints (see fig. S4), TE is plotted for ORFs and for leaders (See SOM for a discussion of leader 'TE' determination) for *IME1*, *CDC28*, and *PDS1*. Values are normalized to the same range for both plots. (**F**) Correlation coefficients [determined from plots as in (E)] were determined for each gene with uORFs for leaders with only near-cognate uORFs and at least one AUG uORF. The positions of six genes that support cap-independent translation (*39*) are noted.

Fig. 5. Regulated transcript extensions expose novel regulatory uORFs. (**A**) mRNA and ribosome occupancy profiles around *SUP35*. (**B**) *ORC1* region displayed as in (A). (**C**) Total RNA from the original timecourse (see fig. S1) was subjected to Northern blotting for *ORC1*. (**D**) Analysis as in Fig. 4E for *ORC1*, *SUP35*, *NDJ1*, *RED1*, *NDC80* and *POP4*. (**E**) Analysis as in Fig. 4F for genes with regulated leader extension (table S5).

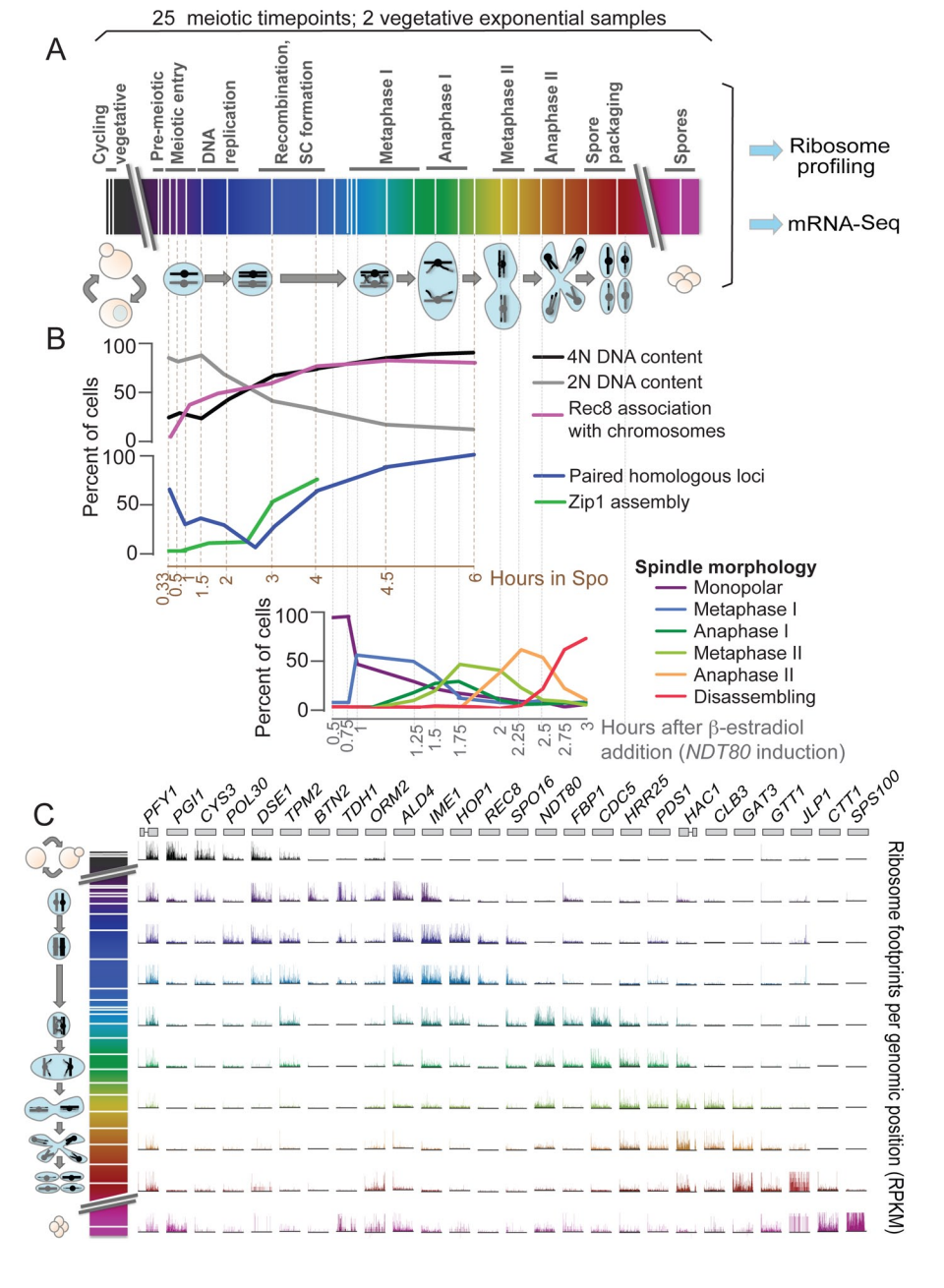
25 meiotic timepoints; 2 vegetative exponential samples
A
Cycling vegetative
Pre-meiotic
Meiotic entry
DNA replication
Recombination, SC formation
Metaphase I
Anaphase I
Metaphase II
Anaphase II
Spore packaging
Spores
Ribosome profiling
mRNA-Seq
B
Percent of cells
4N DNA content
2N DNA content
Rec8 association with chromosomes
Paired homologous loci
Zip1 assembly
Hours in Spo
Spindle morphology
Monopolar
Metaphase I
Anaphase I
Metaphase II
Anaphase II
Disassembling
Hours after β-estradiol addition (NDT80 induction)
C
PFY1
PGI1
CYS3
POL30
DSE1
TPM2
BTN2
TDH1
ORM2
ALD4
IME1
HOP1
REC8
SPO16
NDT80
FBP1
CDC5
HRR25
PDS1
HAC1
CLB3
GAT3
GTT1
JLP1
CTT1
SPS100
Ribosome footprints per genomic position (RPKM)

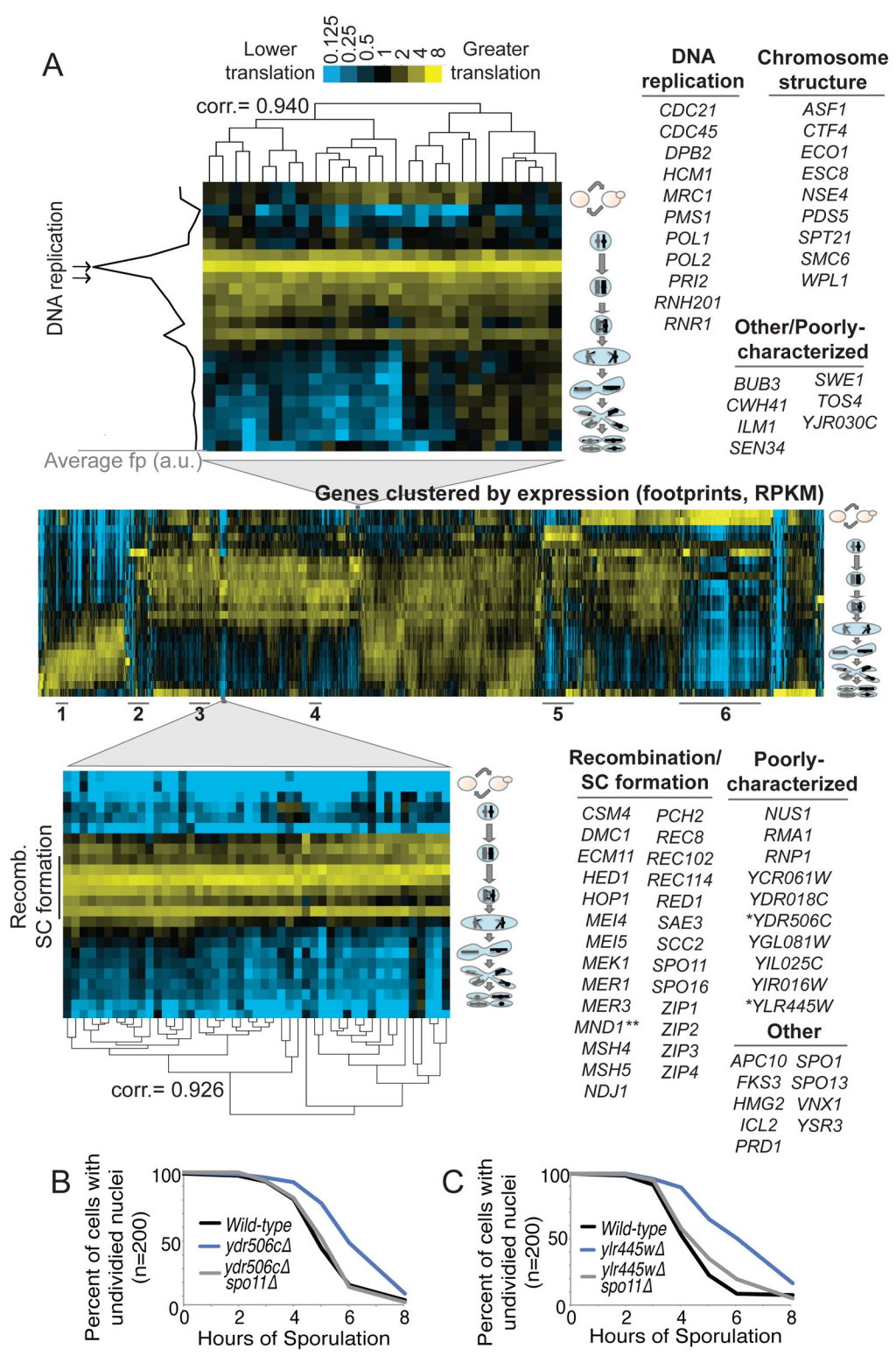
A
Lower translation
0.125
0.25
0.5
1
2
4
8
Greater translation
corr.= 0.940
DNA replication
Average fp (a.u.)
DNA replication
CDC21
CDC45
DPB2
HCM1
MRC1
PMS1
POL1
POL2
PRI2
RNH201
RNR1
Chromosome structure
ASF1
CTF4
ECO1
ESC8
NSE4
PDS5
SPT21
SMC6
WPL1
Other/Poorly-characterized
BUB3
CWH41
ILM1
SEN34
SWE1
TOS4
YJR030C
Genes clustered by expression (footprints, RPKM)
1
2
3
4
5
6
Recomb. SC formation
corr.= 0.926
Recombination/ SC formation
CSM4
DMC1
ECM11
HED1
HOP1
MEI4
MEI5
MEK1
MER1
MER3
MND1**
MSH4
MSH5
NDJ1
PCH2
REC8
REC102
REC114
RED1
SAE3
SCC2
SPO11
SPO16
ZIP1
ZIP2
ZIP3
ZIP4
Poorly-characterized
NUS1
RMA1
RNP1
YCR061W
YDR018C
*YDR506C
YGL081W
YIL025C
YIR016W
*YLR445W
Other
APC10
FKS3
HMG2
ICL2
PRD1
SPO1
SPO13
VNX1
YSR3
B
Percent of cells with undivided nuclei (n=200)
100
50
0
0
2
4
6
8
Hours of Sporulation
Wild-type
ydr506cΔ
ydr506cΔ spo11Δ
C
Percent of cells with undivided nuclei (n=200)
100
50
0
0
2
4
6
8
Hours of Sporulation
Wild-type
ylr445wΔ
ylr445wΔ spo11Δ

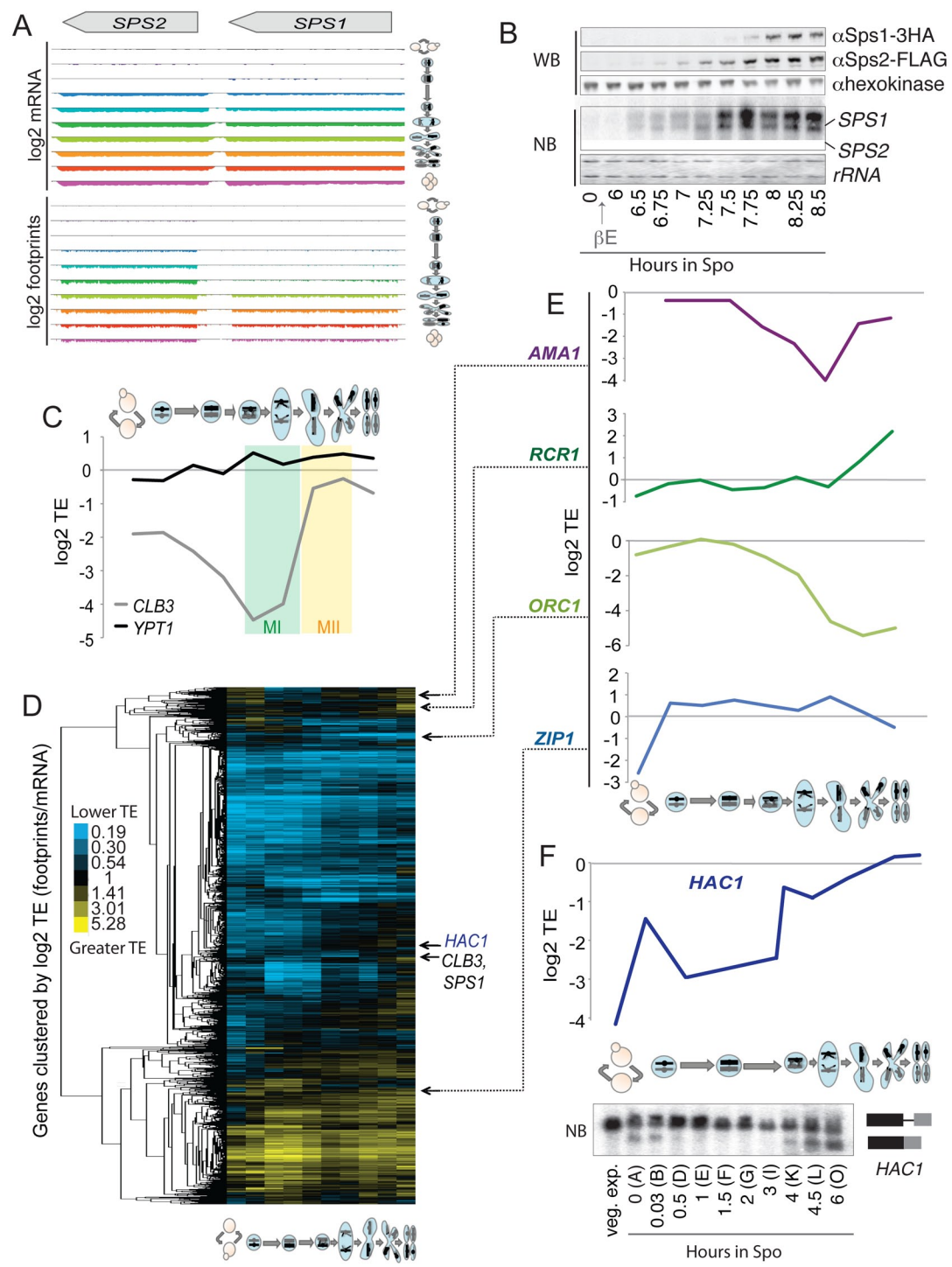
A
SPS2
SPS1
log2 mRNA
log2 footprints
B
WB
αSps1-3HA
αSps2-FLAG
αhexokinase
NB
SPS1
SPS2
rRNA
0
6
6.5
6.75
7
7.25
7.5
7.75
8
8.25
8.5
βE
Hours in Spo
C
log2 TE
CLB3
YPT1
MI
MII
D
Genes clustered by log2 TE (footprints/mRNA)
Lower TE
0.19
0.30
0.54
1
1.41
3.01
5.28
Greater TE
HAC1
CLB3,
SPS1
E
AMA1
RCR1
ORC1
ZIP1
log2 TE
F
HAC1
log2 TE
NB
HAC1
veg. exp.
0 (A)
0.03 (B)
0.5 (D)
1 (E)
1.5 (F)
2 (G)
3 (I)
4 (K)
4.5 (L)
6 (O)
Hours in Spo

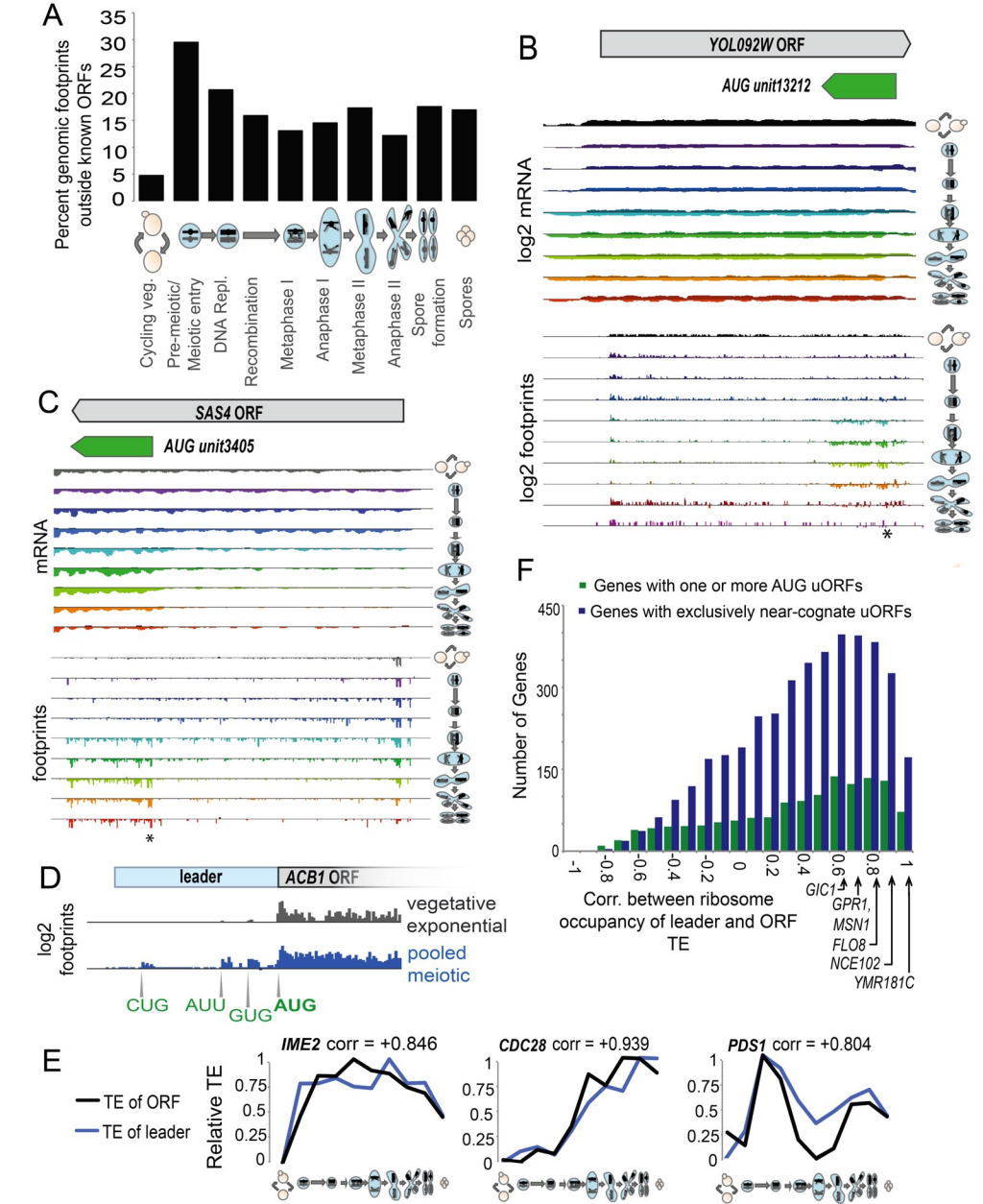
A
Percent genomic footprints outside known ORFs
35
30
25
20
15
10
5
0
Cycling veg.
Pre-meiotic/ Meiotic entry
DNA Repl.
Recombination
Metaphase I
Anaphase I
Metaphase II
Anaphase II
Spore formation
Spores
B
YOL092W ORF
AUG unit13212
log2 mRNA
log2 footprints
C
SAS4 ORF
AUG unit3405
mRNA
footprints
D
leader
ACB1 ORF
log2 footprints
vegetative exponential
pooled meiotic
CUG
AUU
GUG
AUG
E
TE of ORF
TE of leader
Relative TE
IME2 corr = +0.846
CDC28 corr = +0.939
PDS1 corr = +0.804
F
Genes with one or more AUG uORFs
Genes with exclusively near-cognate uORFs
Number of Genes
450
300
150
0
-1
-0.8
-0.6
-0.4
-0.2
0
0.2
0.4
0.6
0.8
1
Corr. between ribosome occupancy of leader and ORF TE
GIC1
GPR1, MSN1
FLO8
NCE102
YMR181C

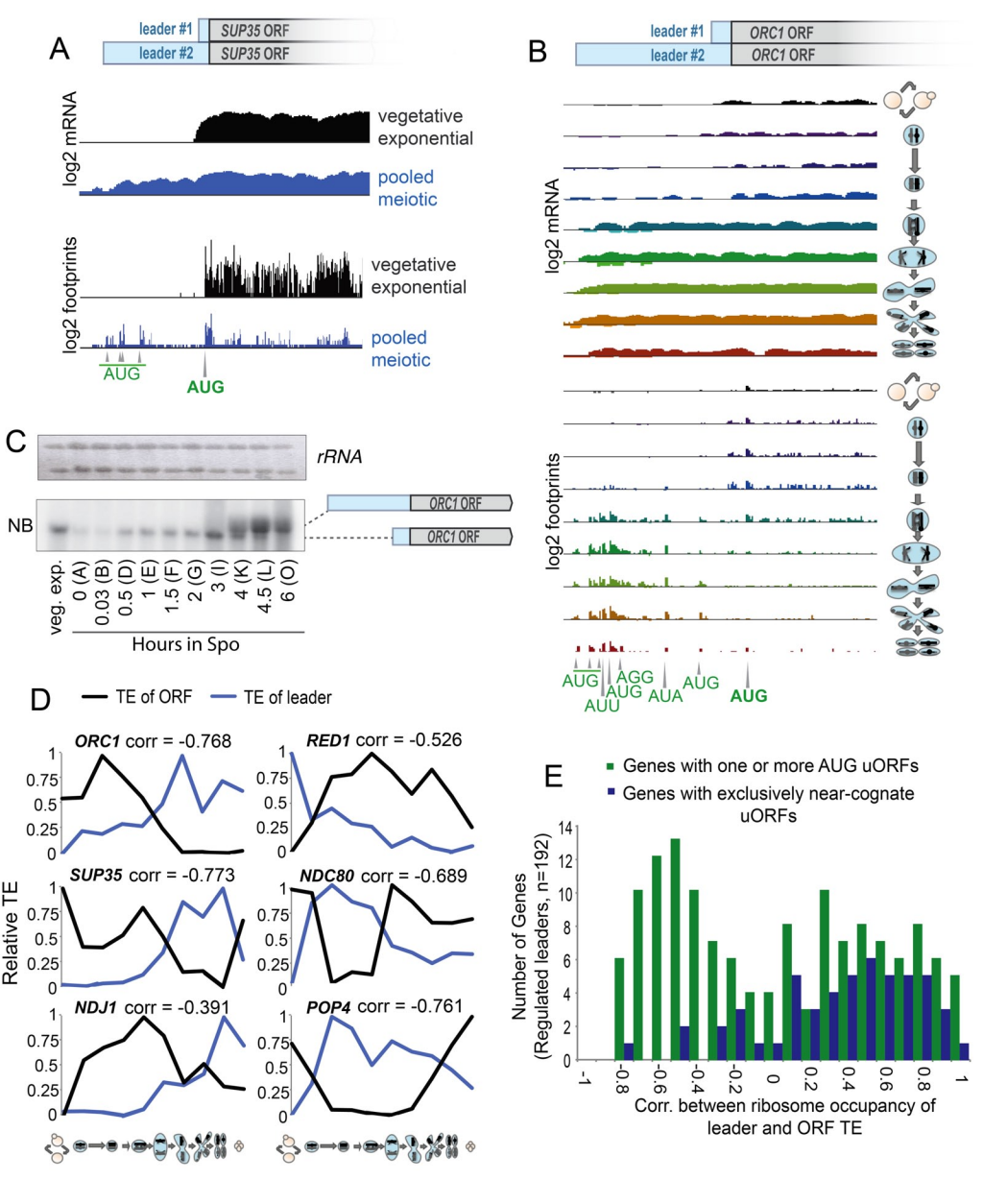
A
leader #1
SUP35 ORF
leader #2
SUP35 ORF
log2 mRNA
vegetative exponential
pooled meiotic
log2 footprints
vegetative exponential
pooled meiotic
AUG
AUG
B
leader #1
ORC1 ORF
leader #2
ORC1 ORF
log2 mRNA
log2 footprints
AUG
AUG
AUU
AGG
AUG
AUA
AUG
AUG
C
rRNA
NB
ORC1 ORF
ORC1 ORF
veg. exp.
0 (A)
0.03 (B)
0.5 (D)
1 (E)
1.5 (F)
2 (G)
3 (I)
4 (K)
4.5 (L)
6 (O)
Hours in Spo
D
TE of ORF
TE of leader
Relative TE
ORC1 corr = -0.768
RED1 corr = -0.526
SUP35 corr = -0.773
NDC80 corr = -0.689
NDJ1 corr = -0.391
POP4 corr = -0.761
E
Genes with one or more AUG uORFs
Genes with exclusively near-cognate uORFs
Number of Genes (Regulated leaders, n=192)
Corr. between ribosome occupancy of leader and ORF TE